CARBON letters

Review Articles
Carbon Letters Vol. 27, 1-11 (2018)

Substitutional boron doping of carbon materials

Sumin Ha[1], Go Bong Choi[1], Seungki Hong[1,2], Doo Won Kim[2] and Yoong Ahm Kim[1,3,♠]

[1]Department of Polymer Engineering, Graduate School, School of Polymer Science and Engineering & Alan G. MacDiarmid Energy Research Institute, Chonnam National University, Gwangju 61186, Korea
[2]Institute of Advanced Composite Materials, Korea Institute of Science and Technology, Jeonbuk 55324, Korea
[3]Institute for Biomedical Sciences, Interdisciplinary Cluster for Cutting Edge Research, Shinshu University, Matsumoto 390-8621, Japan

Article Info

Received 28 October 2017
Accepted 15 November 2017

♠Corresponding Author
E-mail: yak@jnu.ac.kr
Tel: +82-62-530-1871

Open Access

DOI: http://dx.doi.org/10.5714/CL.2018.27.001

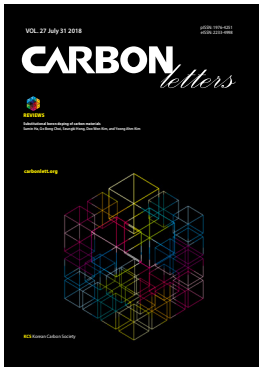

http://carbonlett.org

pISSN: 1976-4251
eISSN: 2233-4998

Abstract

A simple, but effective means of tailoring the physical and chemical properties of carbon materials should be secured. In this sense, chemical doping by incorporating boron or nitrogen into carbon materials has been examined as a powerful tool which provides distinctive advantages over exohedral doping. In this paper, we review recent results pertaining methods by which to introduce boron atoms into the sp^2 carbon lattice by means of high-temperature thermal diffusion, the properties induced by boron doping, and promising applications of this type of doping. We envisage that intrinsic boron doping will accelerate both scientific and industrial developments in the area of carbon science and technology in the future.

Key words: boron atom, substitution, Raman, p-type doping, active site

1. Introduction

Chemical doping with foreign atoms has been the hottest topic given that this method is an effective tool with which to tailor the electronic, mechanical, thermal and chemical properties of various carbon materials, including fullerene, graphite, carbon nanotubes and graphene [1-8]. Experimentally, various methods by which to incorporate the nitrogen atoms into a hexagonal network of graphene have been explored [5-7], as the atomic radius of nitrogen atoms is nearly identical to that of carbon, though with one more electron than carbon. Thus, it is natural to select boron atoms as a promising substitutional doping agent for use with carbon materials, as boron is next to carbon on the periodic table, the atomic radius of boron is close to that of carbon, and boron is trivalent with a coplanar orbital sp^2 structure identical to that of graphene. Therefore, boron-doped carbon materials have garnered much interest because the changes in the electronic and chemical properties of modified carbon materials are expected to be useful. In addition, substitutional boron atoms act as electron acceptors and thus redistribute the π electrons in the sp^2 carbon lattice, thereby depressing the Fermi level and increasing the electron affinity.

Thus far, numerous papers on boron doping have been published [5-7]. It is generally accepted that the exohedrally doped molecules are not stable under extreme conditions, such as those characterized by high humidity, high temperature and high current levels. Considering the effectiveness of intrinsic doping over exohedral doping, this article focuses on the substitutional introduction of boron atoms into the sp^2 carbon lattice. Within this context, this review focuses on the effect of the substitutionally introduced boron atoms on the morphology and physicochemical properties of various carbon materials, including carbon fibers, nanotubes and graphene. The second section describes the method used to introduce boron atoms into the sp^2 carbon lattice via a high-temperature thermal treatment. The third section covers how substitutional boron atoms at the trigonal sites affect the microstructure and physi-

cochemical properties of various carbon materials. The fourth section describes promising applications of boron-doped carbon materials as electrode materials for energy storage devices with an emphasis on how the substitutional boron atoms function.

2. Substitutional Boron Doping into Graphite via High-Temperature Thermal Diffusion

It has been reported that heteroatoms can be introduced into the carbon lattice intentionally via a process defined as "doping." Doping has been used extensively in the past [9,10], mainly to change the distribution of electrons between energy levels in the carbon materials [11] and to affect the graphitization process and modify the chemical state of the surface of the carbon materials. Lowell reported the solid solubility of boron in graphite (ca. 2.35 at% at 2350°C) [9]. It is expected that substitutional boron atoms at the trigonal lattice of graphite are inert because a graphite-like structure with excellent electron delocalization my completely neutralize the boron acidity.

To introduce boron atoms into graphite, highly oriented pyrolytic graphite (HOPG) containing boron carbide was thermally treated at 2500°C for 1 h in argon using a graphite furnace [12]. The topological change caused by boron doping was characterized by scanning tunneling microscopy (STM). Fig. 1 shows the contrast between the STM images of a three-dimensional surface plot with a scan range of 5 nm and the corresponding sectional analysis of pristine HOPG (a) and boron-doped HOPG (b) graphene surfaces. The surface graphene layer of the pristine HOPG with a trigonal lattice shows a perfect superstructure with ABAB stacking, as observed in graphite. On the boron-doped HOPG graphene surface, four substituted B atoms with the highest intensity of the electron groups (Ⓐ–Ⓓ) can be observed in the image. Each bright area consists of boron atoms with the highest electron density levels located in the center of six surrounding medium-intensity sites that correspond to carbon atoms. In addition, the electron density distributions of a substituted boron atom and the surrounding six carbon atoms appear in the three-dimensional surface plot (the inset of Fig. 1b). The substituted boron atom clearly shows the highest electron density in the center. The six carbon atoms closest to the boron atom also show a higher electron density than the next neighboring β-site carbon atoms. This indicates that the substituted boron atoms affect the electronic structure of the six adjacent β-site carbon atoms. The substitution of boron atoms, which are in an electron-deficient state compared to the carbon host, produces vacancies at the top of the valence π-band, resulting in an increase in the density of states near the Fermi level. Due to the enhancement of the density of states, the boron sites become brighter than the surrounding sites in the STM lattice image. This effect is not restricted to boron sites per se but extends to the surrounding carbon sites due to the delocalized nature of the boron-induced defects.

As shown in the inset of Fig. 1a, the closest distance between the β-site carbon atoms observed in the section analysis of the STM image was measured and found to be 0.246 nm for the pristine HOPG. The value is similar to the a_0 spacing in the graphite lattice. On the other hand, the distance between the boron and carbon atoms located at the β-sites is 0.276±0.005 nm, as shown in the inset of Fig. 1b. The distance is slightly longer than the corresponding distance of 0.246 nm in the pristine HOPG. Turbostratic structures are found at the surface of boron-doped HOPG. Some regions show a three-dimensional trigonal image (spot image) of the superstructure (Fig. 1b-I), consistent with ABAB stacking. Some regions are hexagonal (Fig. 1b-II), indicating turbostratic stacking. Thus, the substitution of boron atoms in the hexagonal network affects the stacking nature of the host material, presumably due to the lattice defects and strain associated with the B substitution. Fig. 2 shows a schematic model of boron-substituted graphite. The average distance between the boron and the closest carbon (C1) atoms at the β-sites is 0.276±0.005 nm. The bond distance between the boron and adjacent carbon atoms is calculated to be 0.159 nm, and for the β-site the boron–carbon distance is 0.276 nm. The distance of C1–C1 measured in the STM is also 0.276 nm. The carbon–carbon bond distance at the next β-site was evaluated and found to be identical to that in HOPG (0.246 nm). Therefore, the substituted boron atom may be located at a slightly higher position than the surrounding C atoms along the basal plane of HOPG.

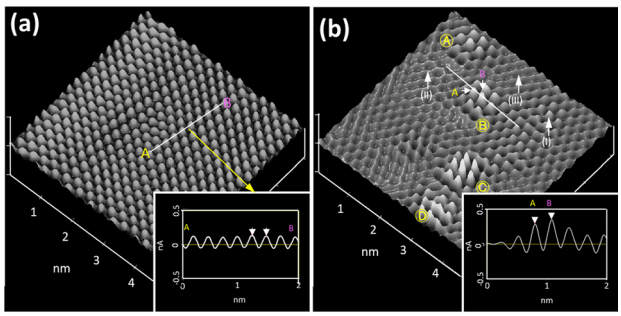

Fig. 1. Scanning tunneling microscopic images of a three-dimensional surface plot (a) and corresponding sectional analysis (b) of a highly oriented boron-doped pyrolytic graphite surface.

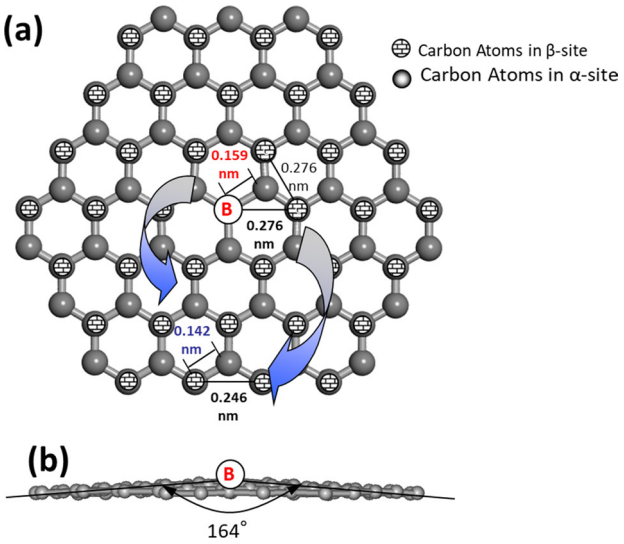

Fig. 2. Schematic models of the top (a) and side (b) view of a boron-substituted graphene sheet based on the measured dimensions of B-C1 and C1-C1.

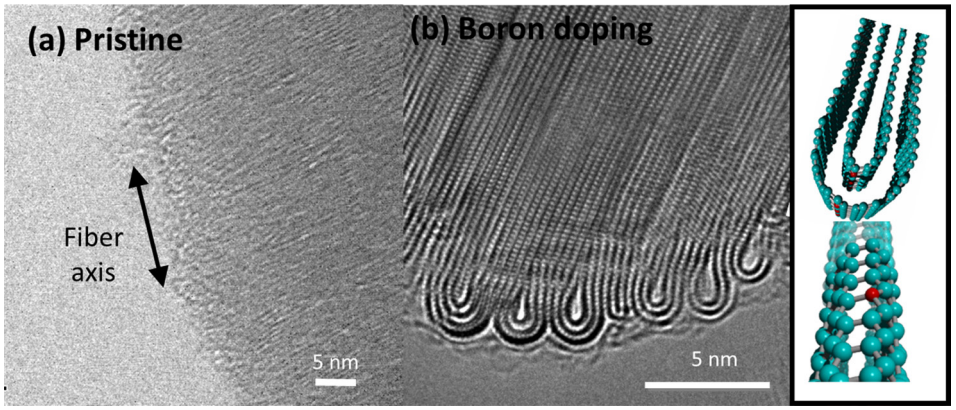

Fig. 3. (a) Transmission electron microscopy (TEM) image of as-grown platelet-type carbon nanofiber. Note that crystalline graphene layers are stacked regularly along the length direction of the carbon nanofiber, the accessible surface of which is covered with active edges. (b) TEM image of boron-doped nanofiber showing multiple stable loops (inset: a schematic model of how boron atoms are introduced into the multi-loop configuration).

The substitution of boron should slightly deform the flatness of the basal plane. Hach et al. [13] reported similar results, showing that the bond distance between boron and carbon atoms is 0.154 nm for $B_2C_4H_6$ and 0.152 nm for $B_2C_52H_{18}$. By restricting the bond length between the B–C atoms obtained from Fig. 1b, the optimized structure of a graphene sheet was simulated. As shown in Fig. 2b, an improper torsion angle (boron at the apex) was calculated and found to be 164°, while the original plane is almost flat with an angle of 179°. It has been reported that the electronic structure is also modified considerably by boron doping, as shown by susceptibility measurements [14]. Thus, both atomically and electronically, the graphite planes could be tailored by B-doping, which can contribute to the ability to modify and control the properties of graphite.

3. How Substitutional Boron Atoms at the Trigonal Sites Affect the Microstructure and Physicochemical Properties

3.1. Platelet-type carbon nanofiber

Carbon materials contain a large number of active edge sites (dangling bonds) that are predominantly present on accessible surfaces; consequently, these active edge sites determine the physical, chemical and electronic properties of the materials [15-18]. For example, the active end planes provide sites for the decomposition of solvated lithium and the subsequent formation of a solid-electrolyte interface [19], resulting in noticeable hysteresis and irreversibility [20]. In order to exploit the intrinsic properties of carbon nanostructures fully and reproducibly, a method capable of controlling their surface characteristics and textures is essential. To date, two methods for modifying edges have been reported: 1) the selective formation of zigzag and armchair edges using Joule heating [21], and 2) the formation of a single loop and multiple loops between adjacent active edges by a high-temperature thermal treatment in argon [22-26]. Alternatively, it has been reported that boron atoms act as a surface modifier [27], as the boron atom is known to replaceable into a hexagonal carbon network. Catalytically grown platelet-type carbon nanofibers were selected as a starting material here, as crystalline graphene layers are stacked regularly along the length direction of the carbon nanofiber and the accessible surface area is covered with active edges. In order to evaluate the effectiveness of boron as a stabilizing agent for open edges (dangling bonds), carbon nanofibers were thermally treated in the presence of elemental boron at various temperatures using a graphite furnace. Thus, it was demonstrated that boron atoms accelerate the loop formation process between energetically unstable (or active) end planes (Fig. 3a), thus resulting in the formation of structurally and electrochemically stable loop-ended surfaces in platelet-type carbon nanofibers (Fig. 3b). Note that the inset in Fig. 3b is a schematic illustration of how boron atoms are introduced into the loop structure substitutionally. In addition, the enhanced electrical conductivity in an individual carbon nanofiber can be explained in terms of the substitutionally introduced B atoms within the loop structure, which covalently connect adjacent parallel graphenes. The enhanced crystallinity, electrical conductivity, and inert loop-ended surface allow B-doped carbon nanofibers to be used as an anode material with high rate capability.

3.2. Single-layer graphene

Micromechanical exfoliation of boron-doped graphite by means of adhesive tape was used to obtain high-quality boron-doped single-layer graphene. The exfoliation step was performed by the repeated folding and unfolding of the tape, which was attached to boron-doped graphite, and the flakes were transferred to a SiO_2/Si substrate. Optical microscope images show graphene flakes at atomic and micrometer thickness levels (Fig. 4a). The Raman maps (Fig. 4c-f) were measured using a 633 nm laser line on optically transparent, large single-layer graphene (as indicated by the arrow in Fig. 4a). Raman maps constitute an efficient method for studying the effects of the number of layers and defects in graphene [28,29]. The boron-doped graphene exhibited two bands characteristic of graphene (Fig. 4b): a G-band at 1580 cm^{-1} corresponding to the stretching vibration of the carbon-carbon bond and a G'-band at 2725 cm^{-1} due to a second-order two-phonon process activated by double reso-

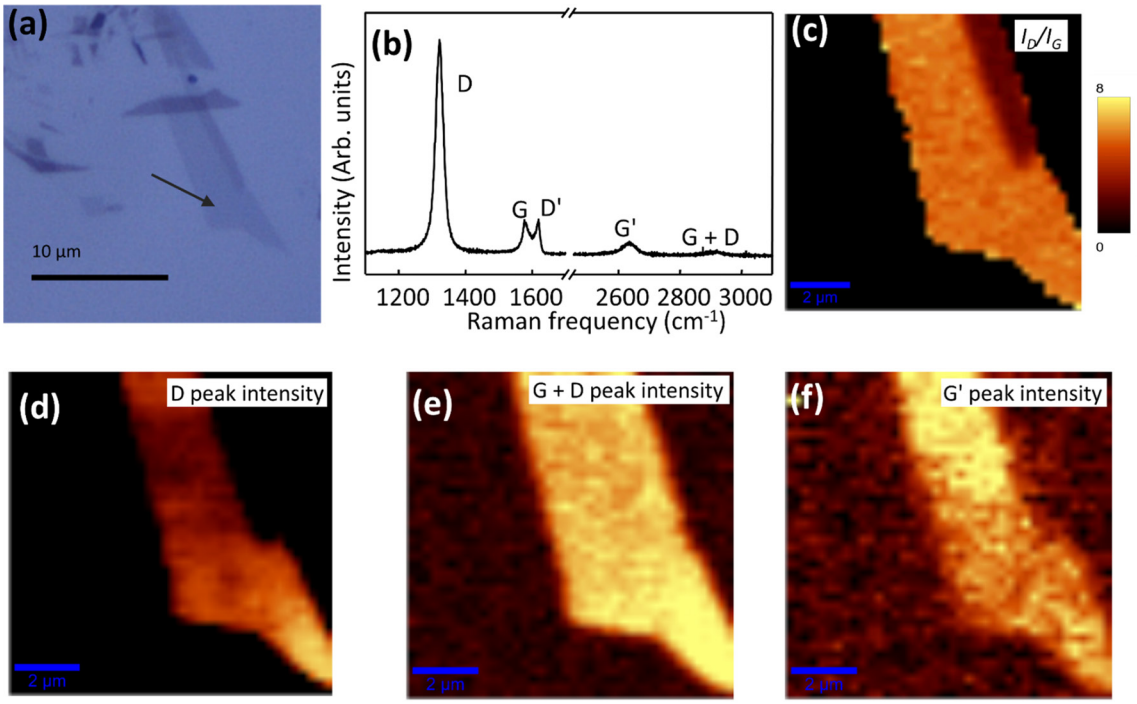

Fig. 4. (a) Optical microscope image of boron-doped single-layer graphene (indicated by the arrow) on an SiO_2/Si substrate, (b) the Raman spectrum obtained using a 633 nm laser line, and spatial maps of (c) ID/IG, the intensities of (d) the D-band, (e) the G + D band, and (f) the G' band. The integrated intensity of the D-band is seven times that of the G-band.

nance processes [30,31]. In addition, three new bands appeared at 1345, 1622 and 2950 cm^{-1} [30,31]; these were attributed to the defect-induced double-resonance Raman feature (the D- and D'-bands) and the combination of G + D (the combination of phonons with different momentum around the Γ and K points). The intensity of the D-band was seven times greater than that of the G-band, and the peak intensity of the D'-band was equal to that of the G-band (Fig. 4b). The low intensity of the D-band in boron-doped graphite indicates strong interaction between the boron and carbon atoms in different layers. More specifically, the scattering amplitude of a photo-excited electron by a boron atom in bilayer graphene is expected to be half of the value that for single graphene because the electronic structure of AB stacked bilayer graphene is either a symmetric or an anti-symmetric combination of wavefunctions of π electrons at the two layers. For multiple layers, because the wavefunction consists of the wavefunctions for various layers, the scattered amplitude becomes inversely proportional to the number of layers. These two bands (e.g., the D and D' bands) are closely associated with the density of defects in graphene [32,33]. However, in order to ensure good structural integrity, the number of defects should be held to a minimum, as the sample was prepared by thermally treating the graphite with a boron compound at 2450°C. Thus, the strong defect-induced peaks (the D- and D'-bands) stem from the chemical disorder of the substitutional boron atoms embedded within the graphene.

Boron-doped single layer graphenes were also prepared by exposing mechanically exfoliated graphenes to microwave plasma containing trimethylborane [34]. Electrical measurements from graphene field-effect transistors revealed that boron-doped graphene exhibited p-type field-effect behavior with on/off ratios exceeding 10^2. Interestingly, the electrical properties were largely dependent upon the number of boron atoms. With an increase in the number of boron atoms, the on/off ratio was increased and the mobility was increased. In addition, the bandgap of graphenes was widened from 0 to 0.54 eV with an increase in the number of boron atoms.

3.3. Metallicity-separated single-walled carbon nanotubes

The effect of substitutional boron doping on the electrical conductivity of a metallicity-separated single-walled carbon nanotube (SWCNT) assembly has been carried out in detail [35]. Metallicity-separated SWCNTs (metallic content >98% (M-SWCNT), semiconducting content >98% (S-SWCNT)) and un-separated SWCNTs were purchased from NanoIntegris Inc. in the form of a sheet (buckypaper). The mean diameter of M-SWCNTs and S-SWCNTs were both 1.4 nm, and the residual catalyst was less than 1 wt% for both the M-SWCNTs and S-SWCNTs. The purity levels of M- and S-SWCNTs were determined by the area ratio of the absorption peaks in the UV–visible spectra. High-temperature boron doping was carried out using a graphite furnace, where the thermal diffusion technique was used to introduce boron atoms into the SWCNT sheets.

Fig. 5 shows the electrical resistivity of the SWCNT sheets as a function of the temperature. For the S-SWCNT sheet, the electrical resistivity was decreased by approximately one order upon

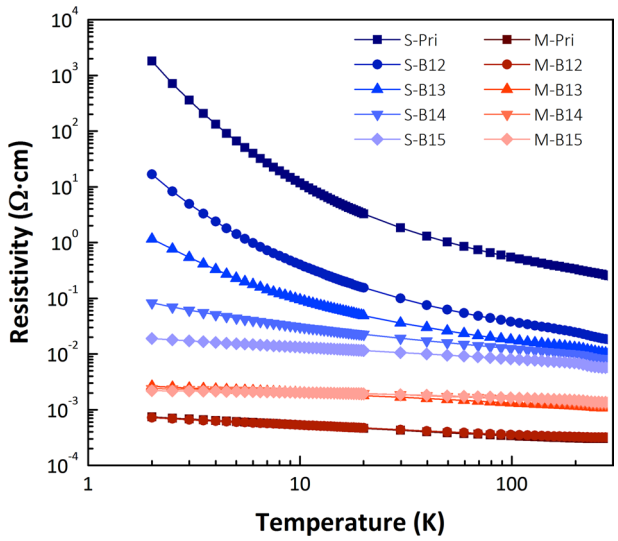

Fig. 5. Resistivity of pristine and boron-doped SWCNT sheets as a function of the temperature. The blue and red curves are obtained from semiconducting and metallic SWCNTs, respectively. The solid lines are guides for the eye.

the introduction of a small amount of boron atoms due to the localized state for hopping conduction. In contrast, we observed an increase in the electrical resistivity upon the boron doping of M-SWCNTs. To evaluate the electrical conduction mechanism quantitatively, the reduced activation energy (W: logarithmic derivative of the resistivity as a function of the temperature) was calculated from the temperature-dependent electrical resistivity. The reduced activation energy is defined by the following equation,

$$W(T) = -\frac{d\ln(\rho(T))}{d\ln(T)}$$

where ρ(T) corresponds to the resistivity at the temperature of T. The reduced activation energy (W) was plotted as a function of the temperature (Fig. 6a). The slope of W was changed by the metallicity and boron doping temperature of the SWCNTs. According to the variable range hopping (VRH) model, the temperature-dependent resistivity follows $\rho(T) = C\exp[(T_0/T)^{1/(d+1)}]$, where C is a constant, T_0 is the characteristic temperature, and d is the dimensionality of hopping [36]. In this case, the slope (p) extracted from the logarithmic W–T plot equals 1/(d+1) (Fig. 6b). Different P-values, in this case P=0.5, 0.33 and 0.25 equal to d=1, 2 and 3, corresponded to the Efros-Shklovskii (ES)-VRH [37], 2D Mott-VRH and 3D Mott-VRH [36] conduction mechanisms, respectively. A W plot (Fig. 6a) and a p plot (Fig. 6b) are generally used to understand the electron transport mechanism in bulk CNT networks [38] as well as the metal–insulator transition behavior in various polymers [39] and complex carbon systems, such as amorphous carbon [40,41], activated carbon fiber [42] and carbide derived carbon [43]. When the p value exceeds 0.25, the conduction mechanism is the hopping mechanism (insulator regime, a strongly localized system). In contrast, when the P-value is lower than 0, the electric conduction mechanism follows the weak localization (WL) theory (metallic regime, a weakly localized system). For S-SWCNTs, for both the S-Pri and S-B12 samples, P equaled approximately 0.5, indicating that the electrons were strongly localized. Therefore, for the S-Pri sample, carriers pass through SWCNT sheets using metallic SWCNT impurities as hopping sites. For S-SWCNTs doped with boron atoms, the ㄱ-value showed a continuous decrease with an increase in the boron doping temperature. For S-B12, substitutional boron atoms created localized states, which contributed to hopping conduction as hopping sites, re-

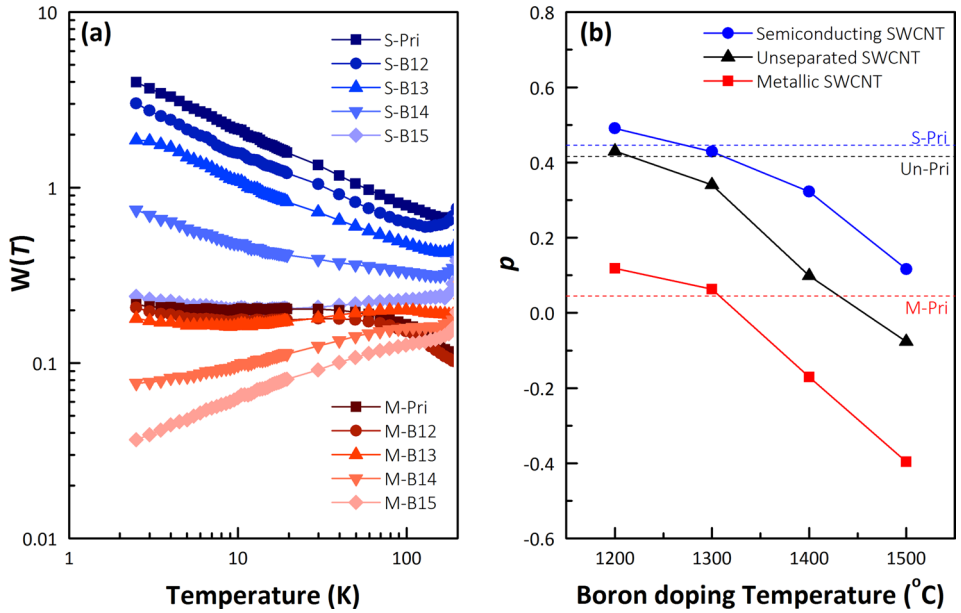

Fig. 6. (a) Reduced activation energy W and (b) the calculated p value from the W plot. The blue, red and black curves are obtained from semiconducting, metallic and unseparated SWCNTs, respectively. The solid lines are guides for the eye.

sulting in a decrease in the electrical resistivity after boron doping. When the boron doping temperature was as high as 1500°C (S-B15), the *P*-value approached 0, indicating that the conduction mechanism changed from VRH (insulator) to WL (metallic). For M-SWCNTs, results similar to the S-SWCNT results were observed. The *P*-value of the boron-doped M-SWCNTs decreased with an increase in the boron doping temperature. For M-B14 and M-B15, the *P*-value was below 0. Therefore, with regard to bulk electrical conduction, electron delocalization was promoted by boron doping for M-B14 and M-B15, whereas the resistivity of the SWCNTs increased after boron doping. The *P*-values for the boron-doped unseparated SWCNT sheets always appeared between the *P*-values of the S-SWCNTs and M-SWCNTs at identical boron doping temperatures.

Finally, the pristine and boron-doped metallic SWCNTs tended to show a decrease in the electrical resistivity in the presence of an external magnetic field perpendicular to the film, which indicated two-dimensional WL behavior. A detailed analysis of the resistivity and the magnetoresistance implied that an increase in inelastic scattering events at the doped boron sites reduced the phase coherence length, leading to an increase in the electrical resistivity.

3.4. Multi-walled carbon nanotubes

An eff ective means of increasing the electrical conductivity of carbon nanotube assemblies is to introduce a large amount of substitutionally doped-boron atoms (ca. 0.496 at%) on the sidewalls of such tubes [44]. A schematic diagram of how substitutional boron atoms are introduced onto the surface of carbon nanotubes is described in Fig. 7. Active oxygen species generated by a vacuum ultraviolet treatment will produce a mild oxidation reaction on the sidewalls of the tubes. Such oxidation-derived defects appear to aid the reaction of nitrogen atoms with the sidewalls of the tubes during the subsequent nitrogen plasma treatment. The nitrogen atoms entrapped within the carbon nanotubes are then desorbed as gases below 1500°C under argon. Such a desorption process may create a number of point defects, which could augment the number of boron atoms occupying the trigonal sites on the sidewalls of the tubes at a relatively low temperature of 2000°C. Thus, the introduction of a large number of boron atoms within the carbon nanotubes increases the carrier concentration, thereby resulting in an overall increase in the electrical conductivity of carbon nanotube films. It is envisaged that our approach will provide a potential solution when using macro-structured nanotube film assemblies in which high electrical transport, high optical transparency and low weights are desirable (e.g., for the fabrication of transparent conductive film and power transmission lines).

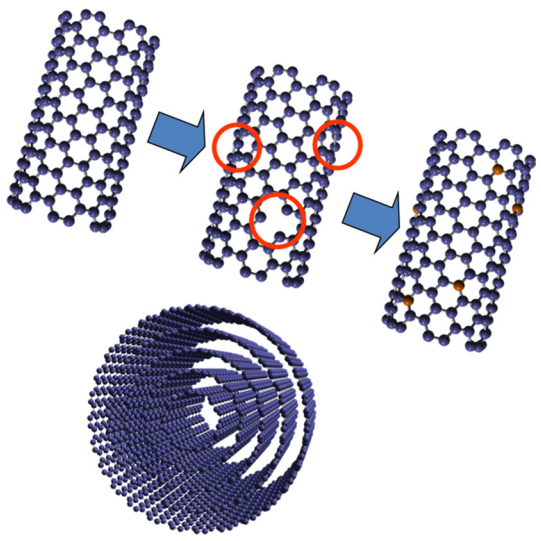

Fig. 7. A schematic illustration of how boron atoms are introduced onto multi-walled carbon nanotubes heavily and substitutionally with the help of defects.

4. Promising Applications of Boron-doped Carbon Materials

4.1. The anode performance of lithium ion batteries

It is generally accepted that boron doping generates electron acceptor levels, thus enhancing the ability to store lithium ions [45]. Graphite powders containing boron carbide were thermally treated at 2500°C in argon using a graphite furnace. Fig. 8 describes the typical voltage profiles of the

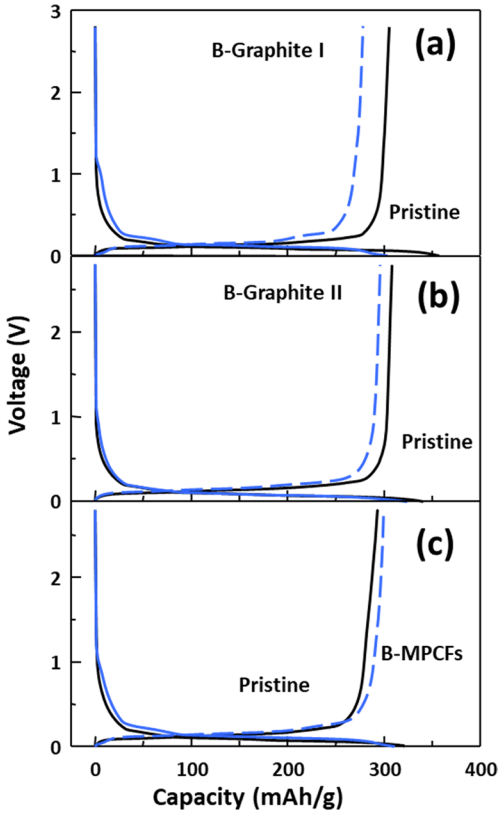

Fig. 8. Change in the potential during the second discharge and charge cycle of graphitized and boron-doped samples for various types of graphite hosts.

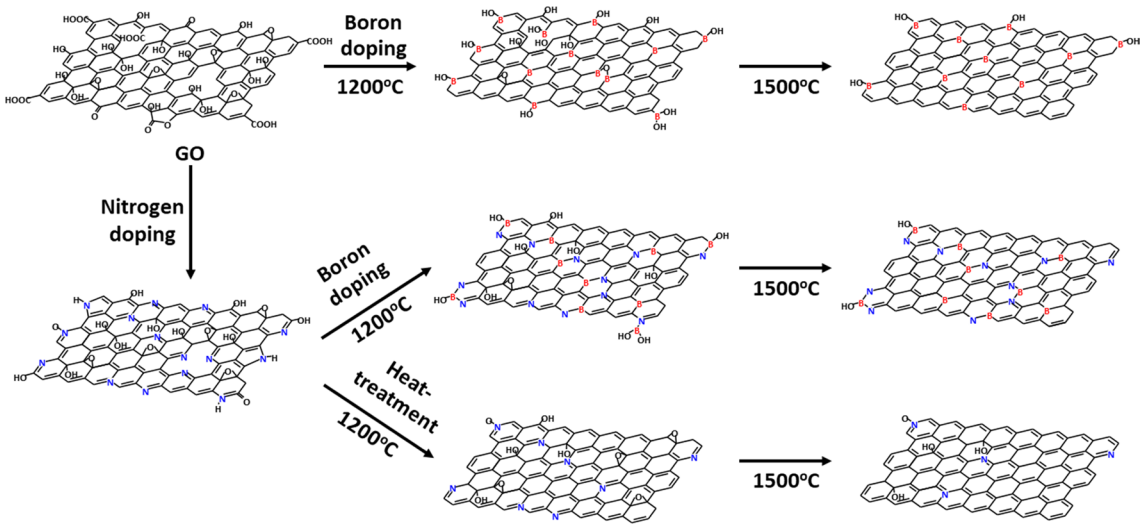

Fig. 9. A schematic illustration of doping behaviors during a nitrogen plasma treatment and the high-temperature thermal diffusion of boron.

second discharge and charge for the B-doped graphite cells. The samples were prepared from a mixture of the pristine material and boron carbide by a heat-treatment at 2800°C in an argon atmosphere. The long plateaus below 0.2 V correspond to the reversible intercalation of Li in the graphitized pristine and the B-doped samples. It should be noted that the second discharge/charge capacities of boron-doped graphitizable carbon I (B-Graphite I, Fig. 8a) and graphitizable carbon II (B-Graphite II, Fig. 8b) were slightly lower than that of the pristine graphite. However, in the case of boron-doped MPCFs, the second charge capacity is larger than that of the undoped pristine (Fig. 8c). The reduced charge capacity of the boron-doped samples may be related to boron atoms occupying the Li insertion active sites, such as edge-type sites in the graphite layers, which would inhibit the Li insertion process. In the discharging cycle of boron-doped samples, negligible shoulder plateaus are characteristically observed at about 1.3 V, which may be caused by the induction of an electron acceptor level such that Li insertion yields a higher voltage compared to undoped samples. It is interesting that the irreversible capacity loss for some boron-doped samples is lower than that of the corresponding undoped samples. These results may be related to the redistribution of the Fermi level of the boron-doped samples, which is lowered by boron doping, that is, by the introduction of an electron acceptor into the lattice.

4.2. Electrodes of supercapacitors

Chemically doped graphene has been actively investigated as an electrode material with which to realize high-performance electrochemical systems. However, the stability of pure-carbon-rich edges and/or heteroatom-decorated edges and their effects on the electrochemical performance remain largely unexplored [46]. It has been observed that during a high-temperature thermal doping process, functionalized graphene edges are structurally stable at 1200°C, whereas the edges at 1500°C are unstable and coalesce into loops through the formation of covalent bonds between adjacent graphenes. A rough schematic doping process (Fig. 9) is proposed for B-, N- and BN- co-doped graphene materials. From X-ray photoelectron spectroscopy (XPS) studies, we concluded that a substantial amount of N and BN or BNO moieties were generated in N-doped and NB-doped graphenes, respectively. For B- and NB-doped graphenes, a large number of boron atoms are present in the form of B-O bonds. It has been reported that boron atoms in carbon lattices show both a catalytic effect and an inhibition effect on carbon oxidation due to the redistribution of π electrons and a reduction in the electron density of the active carbon atom, respectively [47,48]. Therefore, the introduced boron atoms reduce the electron density of active carbon atoms and prevent the chemisorption of an oxygen atom to a carbon atom, thus resulting in the formation of a B-O bond. Moreover, because carbon atoms at edge sites possess higher chemical activity, a large number of boron atoms in the form of a B-O bond must be located at the edges. We believe that the NB co-doping process changes the configuration of boron or nitrogen from BCO to BN and BNO. In addition, the NB co-doping process is expected to stabilize nitrogen atoms as BN or BNO moieties during the high-temperature heat treatment. The substantial decrease in the amount of BNO moieties with an increase in the temperature up to 1500°C can be explained by the thermal evolution of oxygen-related functional groups as well as by structural loop formation at the edges.

Interestingly, boron and nitrogen co-doped graphene prepared at 1200°C showed the largest capacitance in both acidic and an alkaline media due to the presence of BNO moieties along the edge sites. The doped material also showed the best rate capability due to the largely enhanced electrical conductivity originating from the substitutionally doped boron and nitrogen atoms. Our findings regarding the stability of heteroatom-decorated edges without looping formation can now be utilized as a guideline for maximizing the electrochemical activity of graphene in various electrochemical systems.

4.3. Catalytic functions

Numerous studies have been carried out to find alternatives to Pt-based catalysts for oxygen reduction reactions in fuel cells. Thus far, nitrogen-doped and defective carbon materials as metal-free catalysts have attracted considerable amounts of attention due to their high electrocatalytic performance capabilities in fuel cells [49-51]. However, there are rather limited studies on the catalytic effect of boron-doped carbon materials. Sheng et al. [52] synthesized boron-doped graphene by thermally treating graphene oxide in the presence of boron trioxide at 1200°C. They observed that the boron-doped graphenes showed excellent electrocatalytic activity toward oxygen reduction reactions in alkaline electrolytes, highly comparable to the performance of Pt catalysts. Their additional functions are long-term stability and good CO tolerance. However, the mechanism of doped-boron atoms in graphene remains unclarified.

4.4. Supporting materials of Pt in a fuel cell

One of the main hurdles preventing the commercialization of fuel cells is their low long-term stability, especially at high current densities [53]. Possible reasons for the degradation of the electrochemical active surfaces of Pt are as follows: 1) the dissolution of small metal particles and precipitation onto larger ones; 2) migration on the surface of the carbon support and then coalescence into large particles; 3) detachment 4) dissolution and precipitation in the ionomer phase; and 5) the corrosion of the carbon support.

There are two proposed pathways for the corrosion of carbon supports [54].

$$C + 2H_2O = CO_2 + 4H^+ + 4e^-,\ 25°C,\ 0.207\ V\ vs.\ SHE \quad (1)$$

$$C + H_2O = CO + 2H^+ + 2e^-,\ 25°C,\ 0.518\ V\ vs.\ SHE \quad (2)$$

CO is thermodynamically unstable with respect to CO_2, and

$$CO + H_2O = CO_2 + 2H^+ + 2e^-,\ -0.103\ vs.\ SHE. \quad (3)$$

The degradation of both the proton-exchange membrane fuel cell cathode in a potential window of 0.6–1 V and the direct methanol fuel cell anode around 0.4 V is caused by the corrosion of the carbon support [55]. To solve this problem, Acharya and colleagues [56-58] carried out theoretical studies of the binding energy between Pt and a boron-substituted carbon model. The boron atom has a vacant p orbital which can be strongly hybridized with the d orbital of a transitional metal atom. They found that the binding energy between platinum and a one-boron-substituted carbon structure was increased by 0.48 eV relative to an intrinsic carbon reference. In addition, the substituted boron atoms which interacted with the hexachloroplatinate anion prevented the migration and clustering of the platinum particles, resulting in the formation of highly dispersed and small Pt particles. If an appropriate amount of boron atoms is introduced onto carbon materials substitutionally, the durability issue of the fuel cell can be resolved by using boron-doped carbon as a supporting material. It is envisaged that the substitutional boron atoms within carbon materials act as anchoring sites for Pt while also decreasing the degree of carbon corrosion.

4.5. Superconductivity of boron-doped carbon nanotubes

Carbon materials have been among the most desired alternatives to achieve room-temperature superconductivity. Specifically, to achieve a relatively high transition temperature, doping (introduction of foreign atoms) has been examined as a powerful tool to develop a carbon-based superconductor. For example, graphite and fullerene doped with alkali metals showed superconductivity and diamond showed a metal-insulator transition upon the introduction of boron atoms [59-61]. When considering their one-dimensional feature, carbon nanotubes have attracted much attention due to the following reasons: 1) strong coupling interaction between the σ-π electrons and the radial breathing mode in the phonon due to high curvature, and 2) a high electronic density of states due to the alignment of the Fermi level to a van Hove singularity. In this sense, the substitutional introduction of boron element into carbon nanotubes is expected to induce superconducting behavior. Murata et al. [62] observed the Meissner effect at a transition temperature of 13 K from boron-doped SWNT film [63]. The main characteristics of boron-doped SWNT film are that the boron concentration is below 1 at% and the nanotube diameter is less than 1 nm. Based on a theoretical study, they observed a clear relationship between the boron concentration and the Meissner effect for the van Hove singularity. The same group found that the superconducting transition temperature was increased to 19 K by applying pressure to the SWNT film [64]. This work clearly demonstrated the effectiveness of carrier doping for the realization of a high-transition temperature in a carbon-nanotube-based superconductor.

5. Summary and Prospects

In terms of carbon science and technology, it is essential to secure a simple but effective means of tailoring the physical and chemical properties of carbon materials according to their specific applications. In this article, we reviewed a method by which to introduce boron atoms into the trigonal lattice of carbon materials, the doping induced properties, and related promising applications. However, the following points with reference to the science and technology of boron-doped carbon materials should be addressed: first, although scanning tunneling scanning microscopy has been used to observe substitutional boron atoms in graphite, an appropriate analytical tool to evaluate the spatial distribution of substitutionally introduced boron atoms within the sp^2 carbon lattice should be developed. Second, experimentally, substitutional boron doping was carried out by thermally treating a mixture consisting of pristine carbon materials and boron as a precursor at a high temperature exceeding 2000°C in argon. It is well known that the diffusion rate of boron atoms is three time higher than that of carbon atoms above 2000°C [65]. Thus, it is expected that the high mobility of boron atoms within the carbon lattice will induce the formation of point defects. However, it is not easy to differentiate between substitutionally introduced boron atoms and point defects within graphene. For example, Raman results show high sensitivity to structural changes of carbon materials before and after boron

doping. However, it is not clear whether the intensified D band in boron-doped carbon materials stems from substitutional boron atoms or point defects. Third, theoretically, an extremely small amount of substitutional boron atoms in carbon materials clearly modifies their electronic structures. Although XPS has been used as a tool to evaluate the amount of the substitutional boron atoms, its sensitivity is very limited up to 0.02 at%. In addition, the assignment of boron-related moieties within carbon materials remains debatable. Thus, it is essential to develop an appropriate or precise tool with which to evaluate boron atoms substitutionally introduced into carbon materials quantitatively. Finally, when considering the effectiveness of carrier doping on the electrical conductivity of carbon materials, the simultaneous introduction of nitrogen and boron atoms is an interesting option. In this case, nitrogen and boron atoms should be introduced into carbon materials substitutionally while avoiding the formation of BN bonds. Eventually, intrinsic boron doping will largely support the tremendous scientific and industrial progress toward the commercialization of carbon materials.

Conflict of Interest

No potential conflict of interest relevant to this article was reported.

Acknowledgements

Y.A.K. acknowledges the financial support from a grant from the National Research Foundation of Korea (NRF) funded by the Korean government (MSIP) (No. NRF-2017R1A2A1A17069771) and from the Nano · Material Technology Development Program through the NRF funded by the Ministry of Science, ICT and Future Planning of Korea (2016M3A7B4021149).

References

[1] Smalley RE. Doping the fullerenes. ACS Symp Ser, **481**, 141 (1992). https://doi.org/10.1021/bk-1992-0481.ch010.

[2] Duclaux L. Review of the doping of carbon nanotubes (multiwalled and single-walled). Carbon, **40**, 1751 (2002). https://doi.org/10.1016/s0008-6223(02)00043-x.

[3] Ewels CP, Glerup M. Nitrogen doping in carbon nanotubes. J Nanosci Nanotechnol, **5**, 1345 (2005). https://doi.org/10.1166/jnn.2005.304.

[4] Terrones M, Jorio A, Endo M, Rao AM, Kim YA, Hayashi T, Terrones H, Charlier JC, Dresselhaus G, Dresselhaus MS. New direction in nanotube science. Mater Today, **7**, 30 (2004). https://doi.org/10.1016/s1369-7021(04)00447-x.

[5] Wang H, Maiyalagan T, Wang X. Review on recent progress in nitrogen-doped graphene: synthesis, characterization, and its potential applications. ACS Catal, **2**, 781 (2012). https://doi.org/10.1021/cs200652y.

[6] Paraknowitsch JP, Thomas A. Doping carbons beyond nitrogen: an overview of advanced heteroatom doped carbons with boron, sulphur and phosphorus for energy applications. Energy Environ Sic, **6**, 2839 (2013). https://doi.org/10.1039/c3ee41444b.

[7] Deng Y, Xie Y, Zou K, Ji X. Review on recent advances in nitrogen-doped carbons: preparations and applications in supercapacitors. J Mater Chem A, 4, 1144 (2016). https://doi.org/10.1039/c5ta08620e.

[8] Agnoli S, Favaro M. Doping graphene with boron: a review of synthesis methods, physicochemical characterization, and emerging applications. J Mater Chem A, **4**, 5002 (2016). https://doi.org/10.1039/c5ta10599d.

[9] Lowell CE. Solid solution of boron in graphite. J Am Ceram Soc, **50**, 142 (1967). https://doi.org/10.1111/j.1151-2916.1967.tb15064.x.

[10] Kouvetakis J, Kaner RB, Sattler ML, Barlett N. A novel graphite-like material of composition BC_3, and nitrogen–carbon graphites. J Chem Soc Chem Commun, 24, 1758 (1986). https://doi.org/10.1039/c39860001758.

[11] Marchand A. Electronic properties of doped carbons. In: Walker PL, ed. Chemistry and Physics of Carbon, Marcel Dekker, New York, 155 (1971).

[12] Endo M, Hayashi T, Hong SH, Enoki T, Dresselhaus MS. Scanning tunneling microscope study of boron-doped highly oriented pyrolytic graphite. J Appl Phys, **90**, 5670 (2001). https://doi.org/10.1063/1.1409581.

[13] Hach CT, Jones LE, Crossland C, Thrower PA. An investigation of vapor deposited boron rich carbon-a novel graphite-like material–part I: the structure of BCx (C_6B) thin films. Carbon, **37**, 221 (1999). https://doi.org/10.1016/s0008-6223(98)00166-3.

[14] Matthews MJ, Dresselhaus MS, Dresselhaus G, Endo M, Nishimura Y, Hiraoka T, Tamaki N. Magnetic alignment of mesophase pitch-based carbon fibers. Appl Phys Lett, **69**, 430 (1996). https://doi.org/10.1063/1.118084.

[15] Rodriguez NM, Chambers A, Baker RTK. Catalytic engineering of carbon nanostructures. Langmuir, **11**, 3862 (1995). https://doi.org/10.1021/la00010a042.

[16] Terrones H, Hayashi T, Muñoz-Navia M, Terrones M, Kim YA, Grobert N, Kamalakaran R, Dorantes-Dávila J, Escudero R, Dresselhaus MS, Endo M. Graphitic cones in palladium catalysed carbon nanofibres. Chem Phys Lett, **343**, 241 (2001). https://doi.org/10.1016/s0009-2614(01)00718-7.

[17] Endo M, Kim YA, Hayashi T, Fukai Y, Oshida K, Terrones M, Yanagisawa T, Higaki S, Dresselhaus MS. Structural characterization of cup-stacked-type nanofibers with an entirely hollow core. Appl Phys Lett, **80**, 1267 (2002). https://doi.org/10.1063/1.1450264.

[18] Campos-Delgado J, Romo-Herrera JM, Jia X, Cullen DA, Muramatsu H, Kim YA, Hayashi T, Ren Z, Smith DJ, Okuno Y, Ohaba T, Kanoh H, Kaneko K, Endo M, Terrones H, Dresselhaus MS, Terrones M. Bulk production of a new form of sp2 carbon: crystalline graphene nanoribbons. Nano Lett, **8**, 2773 (2008). https://doi.org/10.1021/nl801316d.

[19] Besenhard JO, Winter M, Yang J, Biberacher W. Filming mechanism of lithium-carbon anodes in organic and inorganic electrolytes. J Power Sources, **54**, 228 (1995). https://doi.org/10.1016/0378-7753(94)02073-c.

[20] Béguin F, Chevallier F, Vix-Guterl C, Saadallah S, Bertagna V, Rouzaud JN, Frackowiak E. Correlation of the irreversible lithium capacity with the active surface area of modified carbons. Carbon, **43**, 2160 (2005). https://doi.org/10.1016/j.carbon.2005.03.041.

[21] Jia X, Hofmann M, Meunier V, Sumpter BG, Campos-Delgado J, Romo-Herrera JM, Son H B, Hsieh YP, Reina A, Kong J, Ter-

rones M, Dresselhaus MS. Controlled formation of sharp zigzag and armchair edges in graphitic nanoribbons. Science, **323**, 1701 (2009). https://doi.org/10.1126/science.1166862.

[22] Rotkin SV, Gogotsi Y. Analysis of non-planar graphitic structures: from arched edge planes of graphite crystals to nanotubes. Mater Res Innovations, **5**, 191 (2000). https://doi.org/10.1007/s10019-001-0152-4.

[23] Endo M, Kim YA, Hayashi T, Yanagisawa T, Muramatsu H, Ezaka M, Terrones H, Terrones M, Dresselhaus MS. Microstructural changes induced in "stacked cup" carbon nanofibers by heat treatment. Carbon, **41**, 1941 (2003). https://doi.org/10.1016/s0008-6223(03)00171-4.

[24] Muñoz-Navia M, Dorantes-Dávila J, Terrones M, Hayashi T, Kim YA, Endo M, Dresselhaus MS, Terrones H. Synthesis and electronic properties of coalesced graphitic nanocones. Chem Phys Lett, **407**, 327 (2005). https://doi.org/10.1016/j.cplett.2005.03.095.

[25] Campos-Delgado J, Kim YA, Hayashi T, Morelos-Gómez A, Hofmann M, Muramatsu H, Endo M, Terrones H, Shull RD, Dresselhaus MS, Terrones M. Thermal stability studies of CVD-grown graphene nanoribbons: defect annealing and loop formation. Chem Phys Lett, **469**, 177 (2009). https://doi.org/10.1016/j.cplett.2008.12.082.

[26] Jia X, Campos-Delgado J, Gracia-Espino EE, Hofmann M, Muramatsu H, Kim YA, Hayashi T, Endo M, Kong J, Terrones M, Dresselhaus MS. Loop formation in graphitic nanoribbon edges using furnace heating or Joule heating. J Vac Sci Technol B Microelectron Nanometer Struct Process Meas Phenom, **27**, 1996 (2009). https://doi.org/10.1116/1.3148829.

[27] Fujisawa K, Hasegawa T, Shimamoto D, Muramatsu H, Jung YC, Hayashi T, Kim YA, Endo M. Boron atoms as Loop accelerator and surface stabilizer in platelet-type carbon nanofibers. ChemPhysChem, **11**, 2345 (2010). https://doi.org/10.1002/cphc.201000298.

[28] Ferrari AC, Meyer JC, Scardaci V, Casiraghi C, Lazzeri M, Mauri F, Piscanec S, Jiang D, Novoselov KS, Roth S, Geim AK. Raman spectrum of graphene and graphene layers. Phys Rev Lett, **97**, 187401 (2006). https://doi.org/10.1103/physrevlett.97.187401.

[29] Dresselhaus MS, Jorio A, Hofmann M, Dresselhaus G, Saito R. Perspectives on carbon nanotubes and graphene Raman spectroscopy. Nano Lett, **10**, 751 (2010). https://doi.org/10.1021/nl904286r.

[30] Saito R, Grüneis A, Samsonidze GG, Brar VW, Dresselhaus G, Dresselhaus MS, Jorio A, Cançado LG, Fantini C, Pimenta MA, Souza Filho AG. Double resonance Raman spectroscopy of single-wall carbon nanotubes. New J Phys, **5**, 157 (2003). https://doi.org/10.1088/1367-2630/5/1/157.

[31] Pimenta MA, Dresselhaus G, Dresselhaus MS, Cançado LG, Jorio A, Saito R. Studying Disorder in graphite-based systems by Raman spectroscopy. Phys Chem Chem Phys, **9**, 1276 (2007). https://doi.org/10.1039/b613962k.

[32] Lucchese MM, Stavale F, Martins Ferreira EH, Vilani C, Moutinho MVO, Capaz RB, Achete CA, Jorio A. Quantifying ion-induced defects and Raman relaxation length in graphene. Carbon, **48**, 1592 (2010). https://doi.org/10.1016/j.carbon.2009.12.057.

[33] Cançado LG, Jorio A, Martins Ferreira EH, Stavale F, Achete CA, Capaz RB, Moutinho MVO, Lombardo A, Kulmala T, Ferrari AC. Quantifying defects in graphene via Raman spectroscopy at different excitation energies. Nano Lett, **11**, 3190 (2011). https://doi.org/10.1021/nl201432g.

[34] Tang YB, Yin LC, Yang Y, Bo XH, Cao YL, Wang HE, Zhang WJ, Bello I, Lee ST, Cheng HM, Lee CS. Tunable band gaps and p-type transport properties of boron-doped graphenes by controllable ion doping using reactive microwave plasma. ACS Nano, **6**, 1970 (2012). https://doi.org/10.1021/nn3005262.

[35] Fujisawa K, Hayashi T, Endo M, Terrones M, Kim JH, Kim YA. Effect of boron doping on the electrical conductivity of metallicity-separated single walled carbon nanotubes. Nanoscale, **10**, 12723 (2018). https://doi.org/10.1039/c8nr02323a.

[36] Mott NF. Conduction in Non-crystalline Materials, Oxford University Press, Oxford (1987).

[37] Shklovskii BI, Efros AL. Electronic Properties of Doped Semiconductors, Springer-Verlag, Berlin (1984).

[38] Vavro J, Kikkawa JM, Fischer JE. Metal-insulator transition in doped single-wall carbon nanotubes. Phys Rev B, **71**, 155410 (2005). https://doi.org/10.1103/physrevb.71.155410.

[39] Menon R, Yoon CO, Moses D, Heeger AJ, Cao Y. Transport in polyaniline near the critical regime of the metal-insulator transition. Phys Rev B, **48**, 17685 (1993). https://doi.org/10.1103/physrevb.48.17685.

[40] Kumari L, Prasad V, Subramanyam SV. Effect of iodine incorporation on the electrical properties of amorphous conducting carbon films. Carbon, **41**, 1841 (2003). https://doi.org/10.1016/s0008-6223(03)00172-6.

[41] Kumari L, Subramanyam SV, Eto S, Takai K, Enoki T. Metal–insulator transition in iodinated amorphous conducting carbon films. Carbon, **42**, 2133 (2004). https://doi.org/10.1016/j.carbon.2004.04.019.

[42] Fung AWP, Dresselhaus MS, Endo M. Transport properties near the metal-insulator transition in heat-treated activatedrotect carbon fibers. Phys Rev B, **48**, 14953 (1993). https://doi.org/10.1103/physrevb.48.14953.

[43] Vora PM, Gopu P, Rosario-Canales M, Pérez CR, Gogotsi Y, Santiago-Avilés JJ, Kikkawa JM. Correlating magnetotransport and diamagnetism ofsp2-bonded carbon networks through the metal-insulator transition. Phys Rev B, **84**, 155114 (2011). https://doi.org/10.1103/physrevb.84.155114.

[44] Kim YA, Aoki S, Fujisawa K, Ko YI, Yang KS, Yang CM, Jung YC, Hayashi T, Endo M, Terrones M, Dresselhaus MS. Defect-assisted heavily and substitutionally boron-doped thin multiwalled carbon nanotubes using high-temperature thermal diffusion. J Phys Chem C, **118**, 4454 (2014). https://doi.org/10.1021/jp410732r.

[45] Endo M, Kim C, Nishimura K, Fujino T, Miyashita K. Recent development of carbon materials for Li ion batteries. Carbon, **38**, 183 (2000). https://doi.org/10.1016/s0008-6223(99)00141-4.

[46] Fujisawa K, Cruz-Silva R, Yang KS, Kim YA, Hayashi T, Endo M, Terrones M, Dresselhaus MS. Importance of open, heteroatom-decorated edges in chemically doped-graphene for supercapacitor applications. J Mater Chem A, **2**, 9532 (2014). https://doi.org/10.1039/c4ta00936c.

[47] Ma X, Wang Q, Chen LQ, Cermignani W, Schobert HH, Pantano CG. Semi-empirical studies on electronic structures of a boron-doped graphene layer–implications on the oxidation mechanism. Carbon, **35**, 1517 (1997). https://doi.org/10.1016/s0008-6223(97)00102-4.

[48] Radovic LR, Karra M, Skokova K, Thrower PA. The role of substitutional boron in carbon oxidation. Carbon, **36**, 1841 (1998). https://doi.org/10.1016/s0008-6223(98)00156-0.

[49] Gong K, Du F, Xia Z, Durstock M, Dai L. Nitrogen-doped carbon nanotube arrays with high electrocatalytic activity for oxygen

reduction. Science, **323**, 760 (2009). https://doi.org/10.1126/science.1168049.

[50] Dai L, Xue Y, Qu L, Choi HJ, Baek JB. Metal-free catalysts for oxygen reduction reaction. Chem Rev, **115**, 4823 (2015). https://doi.org/10.1021/cr5003563.

[51] Guo D, Shibuya R, Akiba C, Saji S, Kondo T, Nakamura J. Active sites of nitrogen-doped carbon materials for oxygen reduction reaction clarified using model catalysts. Science, **351**, 361 (2016). https://doi.org/10.1126/science.aad0832.

[52] Sheng ZH, Gao HL, Bao WJ, Wang FB, Xia XH. Synthesis of boron doped graphene for oxygen reduction reaction in fuel cells. J Mater Chem, **22**, 390 (2012). https://doi.org/10.1039/c1jm14694g.

[53] Borup R, Meyers J, Pivovar B, Kim YS, Mukundan R, Garland N, Myers D, Wilson M, Garzon F, Wood D, Zelenay P, More K, Stroh K, Zawodzinski T, Boncella J, McGrath JE, Inaba M, Miyatake K, Hori M, Ota K, Ogumi Z, Miyata S, Nishikata A, siroma Z, Uchimoto Y, Yasuda K, Kimijima K-I, Iwashita N. Scientific aspects of polymer electrolyte fuel cell durability and degradation. Chem Rev, **107**, 3904 (2007). https://doi.org/10.1021/cr050182l.

[54] Kinoshita K. Carbon: Electrochemical and Physicochemical Properties, Wiley, New York (1988).

[55] Casalegno A, Marchesi R. DMFC anode polarization: experimental analysis and model validation. J Power Source, **175**, 372 (2008). https://doi.org/10.1016/j.jpowsour.2007.09.003.

[56] Acharya CK, Turner CH. Stabilization of platinum clusters by substitutional boron dopants in carbon supports. J Phys Chem B, **110**, 17706 (2006). https://doi.org/10.1021/jp063618p.

[57] Acharya CK, Sullivan DI, Turner CH. Characterizing the interaction of Pt and PtRu clusters with boron-doped, nitrogen-doped, and activated carbon: density functional theory calculations and parameterization. J Phys Chem C, **112**, 13607 (2008). https://doi.org/10.1021/jp8034488.

[58] Acharya CK, Turner CH. Effect of an electric field on the adsorption of metal clusters on boron-doped carbon surfaces. J Phys Chem C, **111**, 14804 (2007). https://doi.org/10.1021/jp073643a.

[59] Weller TE, Ellerby M, Saxena SS, Smith RP, Skipper NT. Superconductivity in the intercalated graphite compounds C_6Yb and C_6Ca. Nat Phys, **1**, 39 (2005). https://doi.org/10.1038/nphys0010.

[60] Emery N, Hérold C, d'Astuto M, Garcia V, Bellin C, Marêché, JF, Lagrange P, Loupias G. Superconductivity of Bulk CaC_6. Phys Rev Lett, **95**, 087003 (2005). https://doi.org/10.1103/physrevlett.95.087003.

[61] Ekimov EA, Sidorov V A, Bauer ED, Mel'Nik NN, Curro NJ, Thompson JD, Stishov SM. Superconductivity in diamond. Nature, **428**, 542 (2004). https://doi.org/10.1038/nature02449.

[62] Murata N, Haruyama J, Reppert J, Rao AM, Koretsune T, Saito S, Matsudaira M, Yagi Y. Superconductivity in thin films of boron-doped carbon nanotubes. Phys Rev Lett, **101**, 027002 (2008). https://doi.org/10.1103/physrevlett.101.027002.

[63] Haruyama J, Matsudaira M, Reppert J, Rao A, Koretsune T, Saito S, Sano H, Iye Y. Superconductivity in boron-doped carbon nanotubes. J Supercond Novel Magn, **24**, 111 (2011). https://doi.org/10.1007/s10948-010-0906-6.

[64] Nakamura J, Matsudaira M, Haruyama J, Sugiura H, Tachibana M, Reppert J, Rao A, Nishio T, Hasegawa Y, Sano H, Iye Y. Pressure-induced superconductivity in boron-doped buckypapers. Appl Phys Lett, **95**, 142503 (2009). https://doi.org/10.1063/1.3242016.

[65] Hennig G. Diffusion of boron in graphite. J Chem Phys, **42**, 1167 (1965). https://doi.org/10.1063/1.1696098.